The International Journal of Advanced Manufacturing Technology (2018) 95:3665–3677
https://doi.org/10.1007/s00170-017-1389-4

ORIGINAL ARTICLE

Milling stability prediction and adaptive chatter suppression considering helix angle and bending

Chenxi Wang[1] · Xingwu Zhang[1] · Hongrui Cao[1] · Xuefeng Chen[1] · Jiawei Xiang[2]

Received: 26 July 2017 / Accepted: 13 November 2017 / Published online: 16 December 2017

Abstract
In milling process, chatter is one of the most unfavorable factors, which will reduce surface quality, limit tool life, accelerate tool wear, and decrease machining efficiency. To solve this problem, a great deal of research has been done in milling dynamic modeling and chatter suppression. In this paper, a new milling force calculation method considering helix angle and bending is presented, in which the instantaneous cutting area is calculated in an improved way. The milling dynamic equations are established based on the proposed model, and the stability limit is obtained with semi discretization method (SDM). Results show that tool bending and helix play important roles in stability lobe diagram (SLD). Subsequently, the stability prediction is verified in the milling experiment. Stability analysis can just provide the guidance for selection of milling parameters. In order to get higher efficiency and larger stable region, the time-domain least mean square (LMS) adaptive algorithm is constructed and implemented for chatter suppression in this article. For the sake of applying the method to experiments, the smart toolholder equipped with piezoelectric stack actuators is designed and mounted to a three-axis milling machine. The experimental results show that this method can suppress chatter effectively.

Keywords Helical end mills · Tool bending · Dynamic modeling · Chatter suppression · LMS algorithm

1 Introduction

High-speed milling has been widely used in aerospace, automobiles, molds, and dies because of high efficiency and accuracy. However, as one of the most unfavorable factors, chatter will reduce surface quality, limit tool life, accelerate tool wear, and decrease machining efficiency. Tool life will decrease by 30 to 50% owing to chatter and even 70% with severe chatter [1]. In order to solve this problem, more and more researchers are attracted to milling dynamic modeling and chatter suppression.

In 1907, Taylor et al. [2] started to study chatter and pointed out that when the frequency of cutting force fluctuation is equal to the machine working frequency, chatter will appear. However, as late as the 1950s, Tobias et al. [3] and Tlusty et al. [4] began to reveal that regenerative effect leads to chatter occurance. Early studies about chatter mainly focused on the turning process with one degree of freedom. It was not until 1995 that Altintas et al. [5] put forward the classical milling dynamic model with two degrees of freedom and obtained the stability limit using zero-order approximation (ZOA) method, which was verified by numerical and experimental results. However, in this model, some factors in practical production process are neglected for simplicity, such as helix, runout, process damping, curve toolpath, loss of contact, variable speed effect, and so on. To make up the error from ignored factors, plenty of scholars engaged in this research for more accurate milling dynamic model. For example, Insperger et al. [6] analyzed the influence of tool helix on stability lobe diagram (SLD), which show that there are some instability islands in the flip region for helical mills. Runout effects were incorporated into the milling model by Schmitz et al. [7], which included a discussion of the influence of runout on surface finish, stability, and surface location error. Tang and Liu [8] built the thin-walled plate milling model and analyzed the maximum material removal rate. Tyler et al. [9] considered process damping effect as exciting force and analyzed the process damping stability prediction in milling. Balachandran et al. [10, 11] adopted the numerical simulation to capture the

✉ Xingwu Zhang
xwzhang@mail.xjtu.edu.cn

[1] State Key Laboratory for Manufacturing System Engineering, School of Mechanical Engineering, Xi'an Jiaotong University, Xi'an 710049, People's Republic of China

[2] Zhejiang Provincial Key Laboratory of Laser Processing Robot/Key Laboratory of Laser Precision Processing & Detection, Wenzhou University, Wenzhou 325035, People's Republic of China

interrupted nature of the milling process. Long et al. [12] analyzed the stability of up-milling and down-milling operations with variable spindle speed. Taking effect of material removal on modal parameters into account, Yang et al. [13] developed an efficient method based on structural dynamic modification for in-process workpiece dynamics. In consideration of tool system deflection, Totis et al. [14, 15] put forward a new model for face milling cutter, which introduced a significant correction to the predicted stability borders when the cutter diameter is relatively large in comparison with tooling system overhang. To the author's knowledge, a helical end milling model considering tool bending with small diameter-overhang ratio is not still developed to improve the prediction accuracy, which is often applied to manufacturing of complex-profile products. In this paper, the milling dynamic equations are established based on tool bending and helix effect. Meanwhile, the stability of equations will be analyzed. With these two common factors included, the stability analysis of milling process will be more accurate.

Stability analysis can provide the guidance for selection of milling parameters (spindle speed and axial cutting depth); however, it cannot guarantee the cutting parameters remain constant. The original stable system may lose stabilization owing to the time varying property of cutting process. Active control is an effective method for chatter control, which can satisfy the real-time requirements of the online control system and realize high performance and high efficiency cutting. Through integrating actuators [16] (electrostrictive actuator [17], active magnetic bearing [18, 19], piezoelectric stack [20, 21], and so on) on spindle, the active control system is able to change the dynamics property of machine tool and afford additional forces to offset cutting forces and increase the system stiffness so that the stable cutting region can be expanded. For example, Niels and Verschuren [22, 23] adopted the robust active control method for chatter suppression, which can guarantee the robust stability. Zhang et al. [24] proposed the model predictive control to compensate the system uncertainty for chatter mitigation in milling process with input constraints. Monnin et al. [20, 21] adopted the optimal control algorithm for chatter suppression using active spindle equipped with piezoelectric stacks. Rashid et al. [25] adopted the palletised workholding for milling vibration control with filtered x-least mean square (X-LMS) algorithm. Jia et al. [26] applied filtered X-LMS algorithm to turning chatter control with piezoelectric actuators. Using piezoelectric patch as the actuator, Zhang et al. [27] applied frequency-domain LMS active control method to milling process and suppress chatter vibration energy almost by 50%. Wang et al. [28] proposed the stiffness variation method for chatter suppression, which succeeded in decrease the milling forces by 70.63% and discussed the infulence of stiffness variation parameters on the stability lobe diagram. Dohner et al. [17] proposed the design of integrating actuators into spindle and it worked. However, this would change the spindle structure and require huge costs. In this paper, the time-domain LMS adaptive algorithm with low computational complexity, good convergence, and better stability is employed to mitigate chatter. In order to apply the algorithm to experiments, the smart toolholder equipped with piezoelectric stack actuators is designed and mounted to a three-axis milling machine for chatter suppression, which need not change the spindle structure with simple structures and fewer expenses.

In this article, the milling dynamic model is established based on tool bending and helix effect and the stability analysis is completed. Besides, the time-domain LMS algorithm is employed for chatter suppression using the smart toolholder equipped with piezoelectric stack actuators. The remainder of this paper is arranged as follows: In Sect. 2, the milling dynamic model considering helical end mills bending is introduced in detail and SLD is obtained. In addition, the proposed model is verified by milling tests. Section 3 constructs the LMS adaptive algorithm for chatter mitigation. Subsequently, the experimental verification using piezoelectric stacks as actuators is presented. Finally, several conclusions are drawn in Sect. 4.

2 Milling dynamic model with helical end mill bending

2.1 Classical milling force model

As shown in Fig. 1, the milling process is simplified as a two-DOF stiffness-mass-damping system [5, 29]. Compared with the rigid workpiece, the milling tool can be assumed as

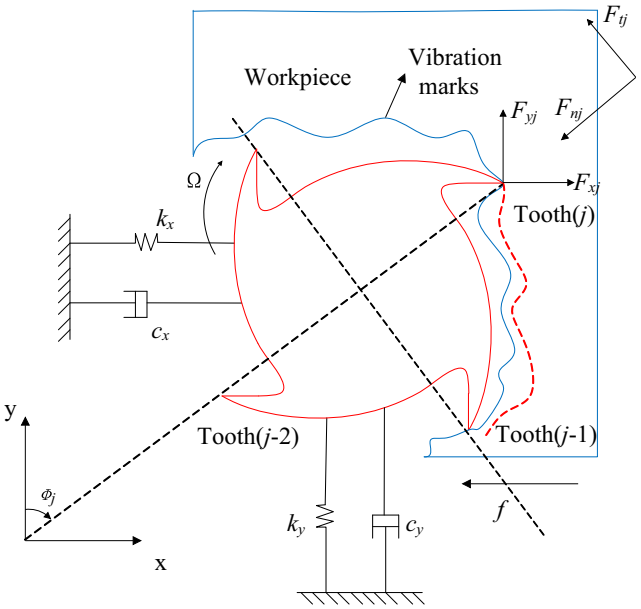

Fig. 1 Schematic representation of milling process

flexible in the x and y directions, where x represents the feed direction and y is perpendicular to the feed direction. The milling forces $[F_x \ F_y]^T$ can be expressed by

$$\begin{bmatrix} F_x \\ F_y \end{bmatrix} = \sum_{j=1}^{N} \begin{bmatrix} F_{xj} \\ F_{yj} \end{bmatrix} \tag{1}$$

where N is the tooth number of milling tool and the helix angle is 0 rad; F_{xj} and F_{yj} are the milling forces of the jth tooth in the x and y directions, respectively.

According to Fig. 1, the F_{xj} and F_{yj} can be written as

$$\begin{bmatrix} F_{xj} \\ F_{yj} \end{bmatrix} = \begin{bmatrix} -\cos(\phi_j(t)) & -\sin(\phi_j(t)) \\ \sin(\phi_j(t)) & -\cos(\phi_j(t)) \end{bmatrix} \begin{bmatrix} F_{tj} \\ F_{nj} \end{bmatrix} \tag{2}$$

where $\phi_j(t) = (2\pi\Omega/60) \times t + (j-1) \times 2\pi/N$ is the angular position of the jth tooth, and Ω is the spindle speed in rpm. F_{tj} and F_{nj} are the tangential and radial milling forces of the jth tooth, respectively. According to the Ref [5], the tangential F_{tj} and radial F_{nj} cutting forces acting on the tooth j are proportional to the axial depth of cut (a) and the instantaneous cutting thickness ($h(\phi_j(t))$), which means that the cutting forces are actually proportional to the instantaneous cutting area ($S_j(t) = ah(\phi_j(t))$)

$$\begin{aligned} \begin{bmatrix} F_{tj} \\ F_{nj} \end{bmatrix} &= \begin{bmatrix} K_t \\ K_n \end{bmatrix} ah(\phi_j(t)) \\ &= \begin{bmatrix} K_t \\ K_n \end{bmatrix} S_j(t) \end{aligned} \tag{3}$$

where the cutting coefficients K_t and K_n are constants. The instantaneous cutting thickness ($h(\phi_j(t))$) can be given by

$$h(\phi_j(t)) = g(\phi_j(t))\left[\Delta x \sin(\phi_j(t)) + \Delta y \cos(\phi_j(t))\right] \tag{4}$$

where $\Delta x = x(t) - x(t-T)$ and $\Delta y = y(t) - y(t-T)$. ($x(t)$, $y(t)$) and ($x(t-T), y(t-T)$)represent the dynamic displacements of the tool at the present and previous tooth periods, respectively. $T = 60/(N\Omega)$ is the tool passing period. $g(\phi_j(t))$ is a screen function and can be described as

$$g(\phi_j(t)) = \begin{cases} 1 & \phi_{st} < \phi_j(t) < \phi_{ex} \\ 0 & otherwise \end{cases} \tag{5}$$

where ϕ_{st} and ϕ_{ex} are the start and exit angles of the tooth j, respectively. For up-milling, $\phi_{st} = 0$ and $\phi_{ex} = \arccos(1 - 2a/D)$, and for down-milling, $\phi_{st} = \arccos(2a/D - 1)$ and $\phi_{ex} = 0$, where a/D is the radial depth of cut ratio.

Substituting Eqs. (2), (3) and (4) into Eq. (1) leads to the classical milling force model with zero helix

$$\begin{bmatrix} F_x \\ F_y \end{bmatrix} = \sum_{j=1}^{N} a \times g(\phi_j(t)) \begin{bmatrix} K_t sc + K_n s^2 & K_t c^2 + K_n sc \\ -K_t s^2 + K_n sc & -K_t sc + K_n c^2 \end{bmatrix} \begin{bmatrix} x(t-T) - x(t) \\ y(t-T) - y(t) \end{bmatrix} \Bigg) \tag{6}$$

where $s = \sin(\phi_j(t))$ and $c = \cos(\phi_j(t))$.

2.2 The bending model of end mills

In milling process, the tool will be subjected to the cutting forces so as to bend as shown in Fig. 2, especially for end milling tool with small diameter-overhang ratio. This phenomenon is also called cutter back-off in the practical production process.

In Fig. 2, XOZ is the Cartesian coordinate, where the original point O is located in the center of tool clamping position; OX and OZ are along the milling tool radial direction and axial direction, respectively. The axial cutting depth is a; the helix angle, overhang, diameter, and teeth number of milling tool are β, L, D, and N, respectively; the milling force is assumed as a uniform force F, where the force at unit length is $Q = F/a$; the elasticity modulus of the milling tool is E. Therefore, according to the calculating formulas [30], the moment of inertia of milling tool can be expressed as

$$I = \frac{\pi {D_1}^4}{64} \tag{7}$$

where D_1 is the equivalent diameter with $D_1 = 0.8D$ considering the effect of milling tool flutes [31].

According to the Euler beam model [30], the flexural displacement and bending angle are respectively

$$\begin{aligned} \Delta x(z) = {} & \frac{Q(L-z)^4}{8EI} - \frac{Qz^2}{24EI}\left(z^2 + 6L^2 - 4zL\right) \\ & + (z + a - L)\tan\left(\frac{Q(L-a)^3}{6EI}\right), \ L - a \le z \le L \end{aligned} \tag{8}$$

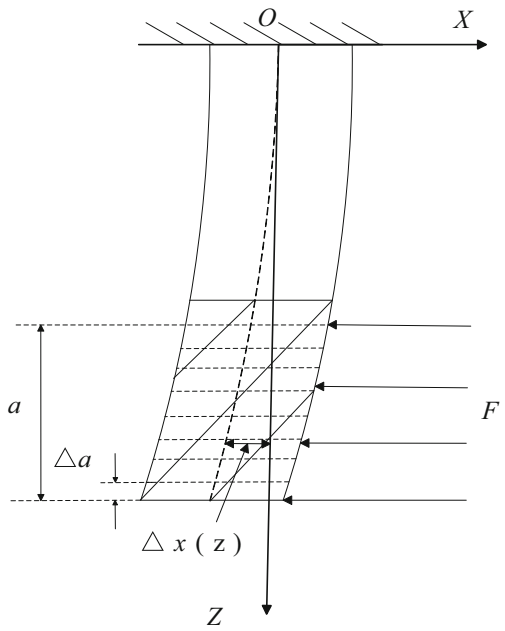

Fig. 2 The bending and helix model of milling tool

$$\theta(z) = \Delta x'(z) = \tan\left(\frac{Q(L-a)^3}{6EI}\right) - \frac{Qz^3}{6EI} - \frac{QzL^2}{2EI} + \frac{QLz^2}{2EI} - \frac{Q(L-z)^3}{2EI}\ ,\ L-a \le z \le L \tag{9}$$

In order to estimate the effect of bending on milling tool, the flexural displacement and bending angle can be calculated with Eqs. (8) and (9). During calculation, the detailed parameters are as follows: $D = 10$ mm, $L = 75$ mm, $a = 10$ mm, $F = 200$ N, and $E = 225$ Gpa. The calculated results show that the maximum flexural displacement and bending angle can reach 1.5 mm and 1.16°, which are large enough to have a certain influence on instantaneous cutting area calculation and milling stability prediction.

2.3 Milling dynamic model with tool bending and helix effect

The milling forces can be calculated by the empirical formulas [32], so the bending angle along the tool axial direction can be obtained. The instantaneous cutting areas at different heights are different due to the tool bending and helix effect. In order to determine the instantaneous cutting area, the milling tool is divided into Na slices along the axial direction as shown in Fig. 2.

An infinitesimal section is taken out for analysis as seen in Fig. 3a, where $dz = \Delta a$ and $\Delta a = a/Na$; $dF = [dF_{tj} \quad dF_{nj}]^T$ is the infinitesimal milling forces including tangential cutting force dF_t and radial cutting force dF_n, which can be expressed as

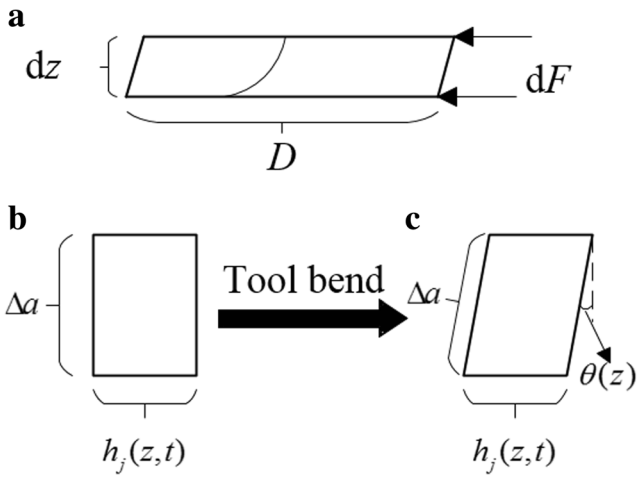

Fig. 3 (**a**) Infinitesimal section of milling tool (**b**) Infinitesimal chip without tool bending (**c**) Infinitesimal chip with tool bending

$$\begin{bmatrix} dF_{tj} \\ dF_{nj} \end{bmatrix} = \begin{bmatrix} K_t \\ K_n \end{bmatrix} \Delta S_j(z,t) \tag{10}$$

where $\Delta S_j(z,t)$ is the instantaneous cutting area of the jth tooth at the height of z with tool bending as seen in Fig. 3c and can be calculated by

$$\Delta S_j(z,t) = \Delta a \times h_j(z,t) \times \cos(\theta(z)) \tag{11}$$

where $h_j(z,t)$ is the instantaneous cutting thickness of the jth tooth at the height of z. In each infinitesimal section, the helix angle can be approximately zero; therefore, $h_j(z,t)$ can be given by

$$h_j(z,t) = g\left(\phi_j(z,t)\right)\left[\Delta x_{jz}\sin\left(\phi_j(z,t)\right) + \Delta y_{jz}\cos\left(\phi_j\left(z,t\right)\right)\right] \tag{12}$$

where $\Delta x_{jz} = x_j(z,t) - x_j(z,t-T)$ and $\Delta y_{jz} = y_j(z,t) - y_j(z,t-T)$. $(x_j(z,t), y_j(z,t))$ and $(x_j(z,t-T), y_j(z,t-T))$ represent the dynamic displacements of the jth tooth at the height of z at the present and previous tooth periods, respectively. $T = 60/(N\Omega)$ is the tool passing period. $\phi_j(z,t)$ indicates the position of the jth tooth at the height of z, which can be expressed by

$$\phi_j(z,t) = (2\pi\Omega/60)t + (j-1)\cdot 2\pi/N - 2(L-z)\tan\beta/D \tag{13}$$

where β and D are the helix angle and diameter of milling tool, respectively. Therefore, the infinitesimal milling forces $[dF_x \quad dF_y]^T$ in the x and y directions can be obtained

$$\begin{bmatrix} dF_x \\ dF_y \end{bmatrix} = \sum_{j=1}^{N} \begin{bmatrix} -\cos\left(\phi_j(z,t)\right) & -\sin\left(\phi_j(z,t)\right) \\ \sin\left(\phi_j(z,t)\right) & -\cos\left(\phi_j(z,t)\right) \end{bmatrix} \begin{bmatrix} dF_{tj} \\ dF_{nj} \end{bmatrix} \tag{14}$$

Substituting Eqs. (10), (11), and (12) into Eq. (14) leads to

$$\begin{bmatrix} \mathrm{d}F_x \\ \mathrm{d}F_y \end{bmatrix} = \sum_{j=1}^{N} g\left(\phi_j(z,t)\right)\cos(\theta(z))\Delta a \begin{bmatrix} K_t sc + K_n s^2 & K_t c^2 + K_n sc \\ -K_t s^2 + K_n sc & -K_t sc + K_n c^2 \end{bmatrix} \begin{bmatrix} x_j(z,t-T) - x_j(z,t) \\ y_j(z,t-T) - y_j(z,t) \end{bmatrix} \tag{15}$$

Accumulate the infinitesimal milling forces $[\mathrm{d}F_x \quad \mathrm{d}F_y]^T$ layer by layer along the axial direction and the total milling forces can be expressed as

$$\begin{bmatrix} F_x \\ F_y \end{bmatrix} = \sum_{i=1}^{Na} \sum_{j=1}^{N} g\left(\phi_j(z,t)\right)\cos(\theta(z))\Delta a \begin{bmatrix} K_t sc + K_n s^2 & K_t c^2 + K_n sc \\ -K_t s^2 + K_n sc & -K_t sc + K_n c^2 \end{bmatrix} \begin{bmatrix} x_j(z,t-T) - x_j(z,t) \\ y_j(z,t-T) - y_j(z,t) \end{bmatrix} \tag{16}$$

where $s = \sin(\phi_j(z,t))$, $c = \cos(\phi_j(z,t))$, $z = L - i \times \Delta a$, and i means the ith infinitesimal section from bottom to top.

A basic milling model with two degrees of freedom is shown in Fig. 1, which can be described by the following equations

$$\begin{bmatrix} m_x & 0 \\ 0 & m_y \end{bmatrix} \begin{bmatrix} \ddot{x} \\ \ddot{y} \end{bmatrix} + \begin{bmatrix} c_x & 0 \\ 0 & c_y \end{bmatrix} \begin{bmatrix} \dot{x} \\ \dot{y} \end{bmatrix} + \begin{bmatrix} k_x & 0 \\ 0 & k_y \end{bmatrix} \begin{bmatrix} x \\ y \end{bmatrix} = \begin{bmatrix} F_x(t) \\ F_y(t) \end{bmatrix} \tag{17}$$

where the terms $m_{x,y}$, $c_{x,y}$, $k_{x,y}$, and $F_{x,y}$ are the modal mass, damping, spring stiffness, and cutting forces in the flexible directions of the system.

Substituting Eq. (16) into Eq. (17) gives milling dynamic equation with tool bending and helix effect

$$\mathbf{M}\ddot{\mathbf{X}}(t) + \mathbf{C}\dot{\mathbf{X}}(t) + \mathbf{K}\mathbf{X}(t) = \mathbf{K}_c[\mathbf{X}(t-T) - \mathbf{X}(t)] \tag{18}$$

where $\mathbf{X}(t) = [x(t) \quad y(t)]^T$ is the two-element position vector; $\mathbf{M}$, $\mathbf{C}$, and $\mathbf{K}$ are the 2×2 modal mass, damping, and stiffness matrices. $\mathbf{K}_c$ is the dynamic cutting coefficients, which can be described as

$$\mathbf{K}_c = \begin{bmatrix} h_{xx}(t) & h_{xy}(t) \\ h_{yx}(t) & h_{yy}(t) \end{bmatrix} \tag{19}$$

where $h_{xx}(t)$, $h_{xy}(t)$, $h_{yx}(t)$, and $h_{yy}(t)$ can be given by

$$h_{xx}(t) = \sum_{i=1}^{Na} \sum_{j=1}^{N} g\left(\phi_j(z,t)\right)\cos(\theta(z))\Delta a\left[K_t sc + K_n s^2\right] \tag{20}$$

$$h_{xy}(t) = \sum_{i=1}^{Na} \sum_{j=1}^{N} g\left(\phi_j(z,t)\right)\cos(\theta(z))\Delta a\left[K_t c^2 + K_n sc\right] \tag{21}$$

$$h_{yx}(t) = \sum_{i=1}^{Na} \sum_{j=1}^{N} g\left(\phi_j(z,t)\right)\cos(\theta(z))\Delta a\left[-K_t s^2 + K_n sc\right] \tag{22}$$

$$h_{yy}(t) = \sum_{i=1}^{Na} \sum_{j=1}^{N} g\left(\phi_j(z,t)\right)\cos(\theta(z))\Delta a\left[-K_t sc + K_n c^2\right] \tag{23}$$

2.4 Milling process stability analysis

Based on the Eq. (18) with semi discretization method (SDM) [33], the proposed stability limit is obtained as the red line in Fig. 4, while the black represents the original stability limit. The simulation parameters are as follows: $N = 3$, $K_t =$

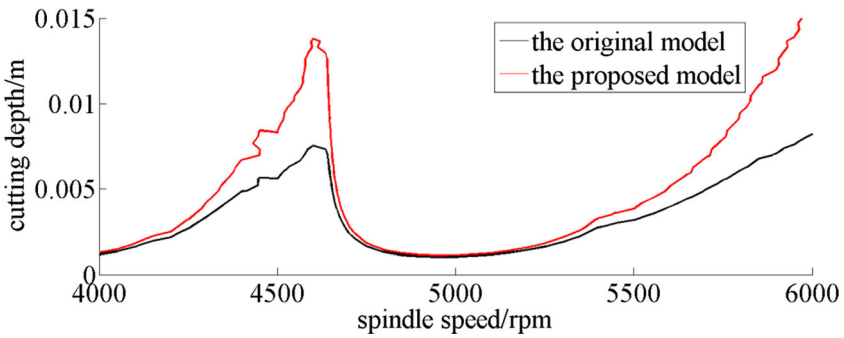

Fig. 4 Stability lobe diagram in milling process

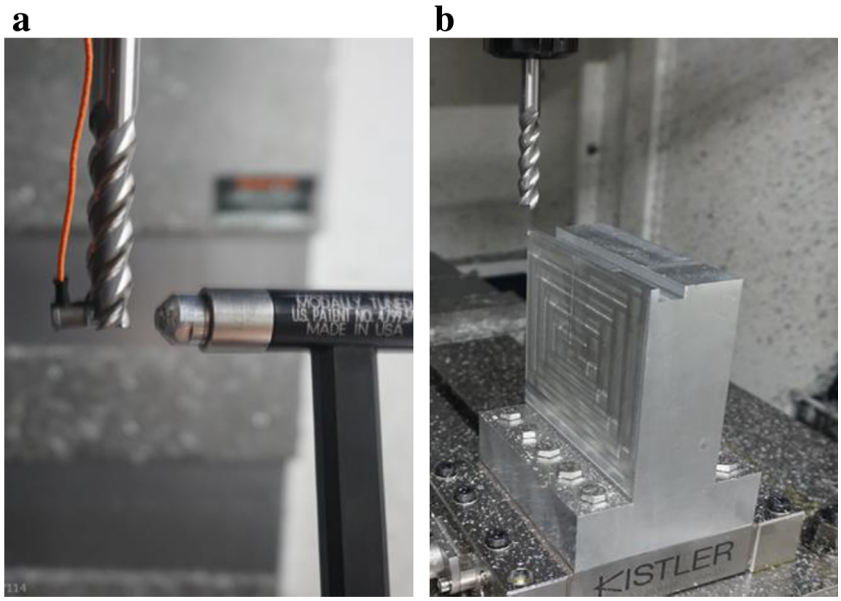

Fig. 5 (a) The impact experiment set-up (b) Milling force measuring set-up

600 Mpa, $K_n = 200$ Mpa, $\omega_{nx} = \omega_{ny} = 922 \times 2\pi$, $m_x = m_y = 0.03993$ kg, $a_e/D = 0.05$, $a = 10$ mm, damping ratio $\xi_x = \xi_y = 0.011$, and up-milling is adopted. It can be known that the proposed stable area is larger than the original especially around the peak, because $dz \times \cos(\theta(z))$ with tool bending is less than dz. From the figure, it can be also known that the increases of SLD are different for different spindle speeds. The higher the critical stability limits are, the more the critical stability limits increase. It can be explained as the following: for the low critical stability limits, the axial cutting depth is low so that the milling forces will be small, which will cause the bending of milling tool to be little. Therefore, the SLD change little in the low critical stability limits areas. However, the larger milling tool bending within high critical stability limits will increase the SLD obviously.

2.5 Experimental verification

In order to verify the influence of tool bending on SLD, three kinds of tests, including impact tests, milling coefficients identification tests, and cutting tests, are implemented on a three-axis milling machine (VMC-V5). A three-flute high-speed steel end mill, with 10 mm diameter, 45° helix angle, and 75 mm overhang, is adopted in the experiment. The workpiece material is aluminum alloy 6061 with elastic modulus of 68.9 GPa, density of 2690 kg/m^3, and Poisson's ratio of 0.33.

2.5.1 Impact tests and milling force coefficient identification tests

The impact tests are implemented with a modal impact hammer (PCB 086C01 with sensitivity 2.25 mV/N) and a microaccelerometer (DYTRAN 3032A with sensitivity 10.00 mV/g) as seen in Fig. 5a. LMS SCADASIII data acquisition system is used to acquire impact forces and acceleration signals with sampling frequency 10,240 Hz. The main modal parameters are analyzed by the PolyMAX module, which are shown in Table 1.

The milling forces are measured by a Kistle 9129A dynamometer for coefficients identification with solt milling, spindle speed 5000 rpm, axial depth 1 mm,

Table 1 Results of modal parameter identification

Modal parameters	Modal mass (kg)	Damp ratio (%)	Natural frequency (Hz)
x direction	0.01154	1.8072	1350.23
y direction	0.01199	0.7126	1349.15

Table 2 Results of force coefficient identification

Milling force coefficients	Tangential (MPa)	Radial (MPa)
Value	560.366	311.657

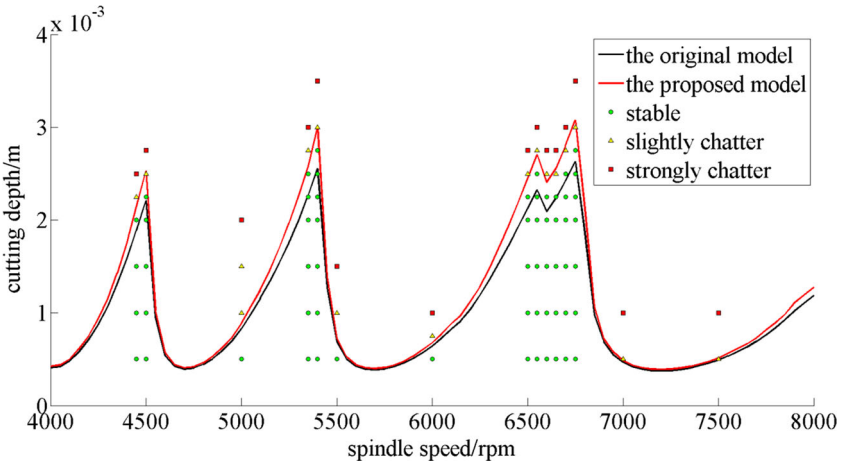

Fig. 6 Comparison between experimental and predicted stability lobes

and sampling frequency 6000 Hz under different feeds per tooth as seen in Fig. 5b. With the identification equations [31], the milling force coefficients are shown in Table 2.

2.5.2 Cutting tests for SLD validation

With the modal parameters in Table 1 and cutting force coefficients in Table 2, the SLD in this cutting condition can be obtained as seen in Fig. 6, where the radial cutting depth is 0.5 mm and the feed per tooth is 0.05 mm/tooth. In order to verify the SLD, a series of milling tests with different cutting parameters are performed. The spindle speed increases from 4000 to 8000 rpm. At each rotating speed, the axial cutting depth increases from 0.5 mm until strongly chatter occurs. The acceleration signals are acquired by LMS SCADASIII data acquisition system with sampling frequency 10,240 Hz through the accelerometer (IMI 608A11 with sensitivity 100 mV/g).

In tests, three statuses appear, including stable, slightly chatter and strongly chatter, where the axial cutting depth of slightly chatter can be used as the critical limit. The acceleration signals in the time and frequency domain under these three statuses are shown in Fig. 7. Here, the spindle speed is 4500 rpm; therefore, the rotational frequency is 75 Hz. In Fig. 7a, there are only the rotational frequency and its frequency multiplication, which means stable cutting. However, besides the frequencies related to spindle speed, the chatter frequencies arise as seen in Fig. 7b, c. The amplitude of chatter frequency in Fig. 7b is much lower than that in Fig. 7c, which can be used to distinguish the slightly and strongly chatter.

Based on the analysis of acceleration signals, the results are shown in Fig. 6, the circle, triangle, and square represent stable, slightly chatter, and strongly chatter, respectively. From Fig. 6, it can be known that the proposed method has better accuracy for stability prediction in milling.

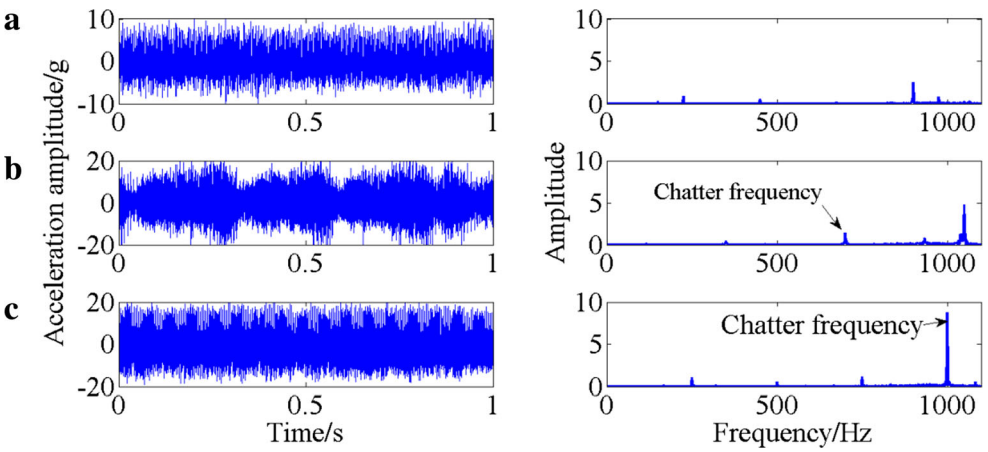

Fig. 7 The acceleration signals in the time and frequency domain. **a** Stable. **b** Slightly chatter. **c** Strongly chatter

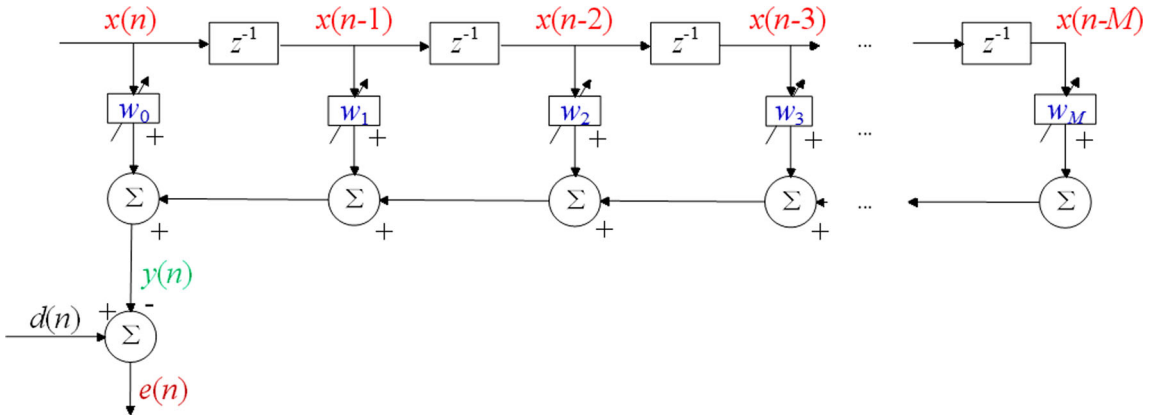

Fig. 8 The adaptive filter

3 LMS adaptive algorithm for chatter active control

The accurate prediction of SLD can just guide for cutting parameters selection; however, it cannot guarantee that the cutting parameters remain constant and the original stable system may lose stabilization owning to the time varying property of cutting process. In ordert to suppress chatter better, the LMS adaptive algorithm is constructed and performed in this section.

3.1 LMS adaptive algorithm

As seen in Fig. 8, the algorithm is really based on a filtering method and the length of filter is assumed as M, where $\mathbf{X}(n) = [x(n), x(n-1), \ldots, x(n-M)]^T$ and $\mathbf{W}(n) = [w_0, w_1, \ldots, w_M]^T$ are input vector and weight vector, respectively; $d(n)$ and $y(n)$ are the ideal output and real output; $e(n)$ is the error output, which can be used as the control signal; and n stands for current time.

The adaptive filter can make the output to track and tend to be the ideal value. In chatter control, the output is supposed to be zero, namely, $d(n)$ is to be zero. From Fig. 8, the real output can be written as

$$y(n) = \sum_{m=0}^{M} w_m x(n-m) \tag{24}$$

simplified as the matrix form

$$y(n) = \mathbf{X}^T(n)\mathbf{W}(n) \tag{25}$$

Therefore, the error $e(n)$ is

$$e(n) = d(n) - \mathbf{X}^T(n)\mathbf{W}(n) \tag{26}$$

To minimize the error $e(n)$, the LMS adaptive algorithm is selected with many advantages, such as low computational complexity, good convergence, and better stability. With LMS adaptive algorithm, the weight can be updated by

$$\mathbf{W}(n+1) = \mathbf{W}(n) - \mu\nabla(n) \tag{27}$$

where μ is the convergence factor. The larger μ is, the faster convergence is. However, when μ is more than a limited value, the iteration is diverging. $\nabla(n)$ is the error

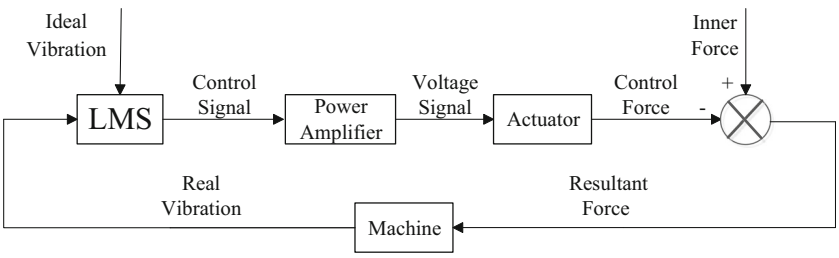

Fig. 9 Control block of chatter in milling process

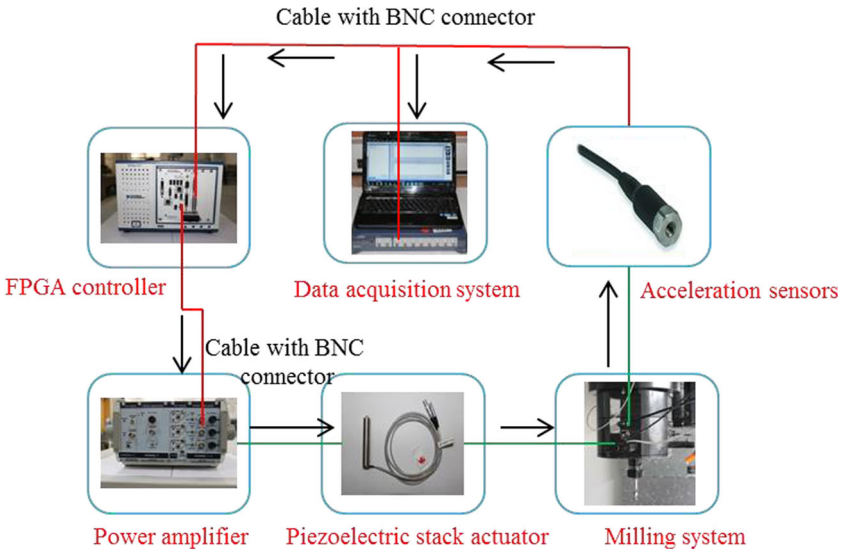

Fig. 10 The setup of milling tests

gradient, which can be defined as

$$\nabla(n) = \begin{bmatrix} \frac{\partial e^2(n)}{\partial w_0} \\ \vdots \\ \frac{\partial e^2(n)}{\partial w_M} \end{bmatrix} = 2e(n) \begin{bmatrix} \frac{\partial e(n)}{\partial w_0} \\ \vdots \\ \frac{\partial e(n)}{\partial w_M} \end{bmatrix} = -2e(n)\mathbf{X}(n) \quad (28)$$

Substituting Eq. (28) into Eq. (27) leads to

$$\begin{aligned} \mathbf{W}(n+1) &= \mathbf{W}(n) - \mu\nabla(n) \\ &= \mathbf{W}(n) + 2\mu \cdot e(n)\mathbf{X}(n) \end{aligned} \quad (29)$$

Equation (29) is the iterative formula of weight vector $\mathbf{W}(n)$ in control process.

In milling process, due to the time varying characteristics of parameters, it will be apt to chatter without real-time control. In order to mitigate chatter better, LMS adaptive algorithm is much needed to track the varying vibration signals and then generate control signals to the actuators, which can produce control forces to offset the cutting forces and increase the system stiffness; thus, chatter can be suppressed.

The control block diagram is shown in Fig. 9. During control process, the machine vibration signals are used as the

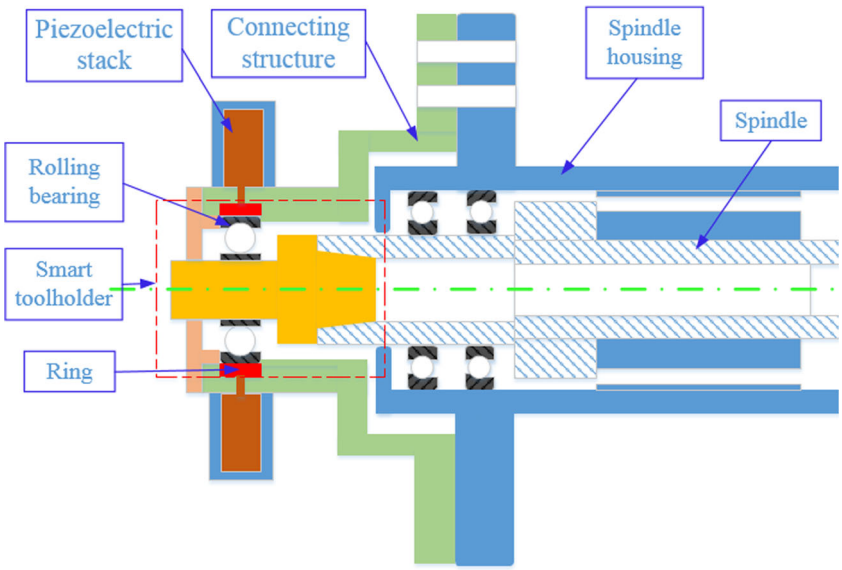

Fig. 11 The schematic diagram of smart toolholder

Fig. 12 The designed toolholder

input of LMS algorithm. The LMS adaptive algorithm can process the machining vibration signals and then output the control signals to the actuators over a power amplifier. Next, the actuators provide the control forces to offset the inner time-varying cutting forces. Finally, the resultant forces act on the machine and cause the vibration signals. The four steps build up a complete closed-loop control frame and can be applied in engineering practices.

3.2 Experimental verification of LMS algorithm

3.2.1 Introduction of experimental setup

The experimental setup of the control process is made up of six parts: the three-axis milling machine (VMC-V5) equipped with smart toolholder, acceleration sensors (IMI 608A11 with sensitivity 100 mV/g), data acquisition system, FPGA controller, power amplifier, and piezoelectric stack actuators as shown in Fig. 10, where the arrows indicate the direction of the signal or data flow. In control process, the PXI-7853R FPGA is chosen as the controller owing to its real-time performance. The LMS active control algorithm is programmed by Labview and downloaded to the FPGA controller. The piezoelectric stack (80VS15, Pst) has the following detailed parameters: maximum displacement 95 μm and maximum output force 2300 N. A power amplifier (Pst E01 B4) is used to enlarge the control signals from FPGA to the actuators. In order to display and record the vibration signal, the data acquisition system, including Dell N4110 and AVANT MI-7008, is used for data sampling with sample frequency 10,240 Hz. In theory, the control forces from piezoelectric stacks are supposed to be the opposite direction to milling forces, which can offset the milling forces and increase the system stiffness for chatter suppression.

3.2.2 Introduction of the smart toolholder equipped with piezoelectric stacks

In order to suppress chatter, the smart toolholder is designed using piezoelectric stacks as actuators. The schematic diagram of smart toolholder is shown in Fig. 11. The piezoelectric stack actuators are used to produce the controlling forces for

Fig. 13 The machining setup

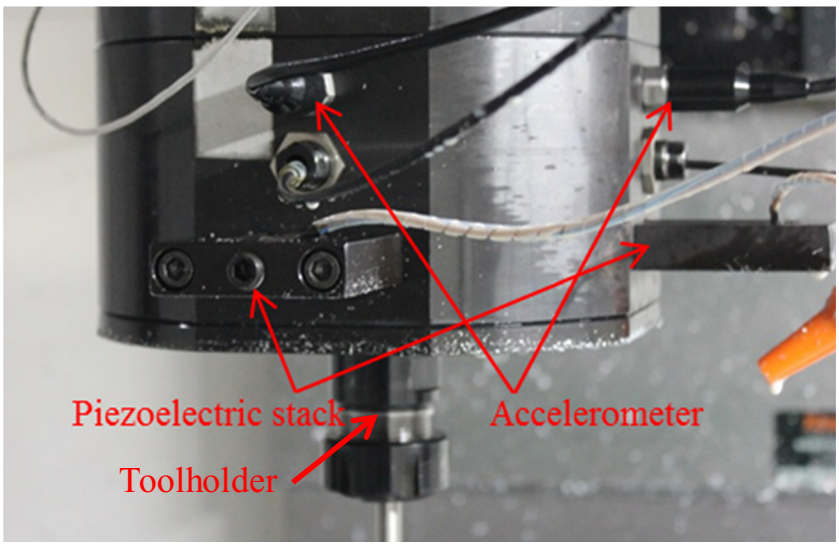

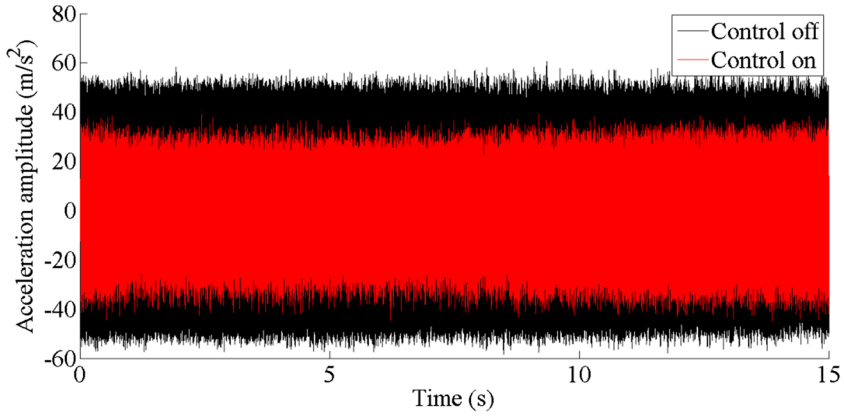

Fig. 14 The acceleration signals in time domain

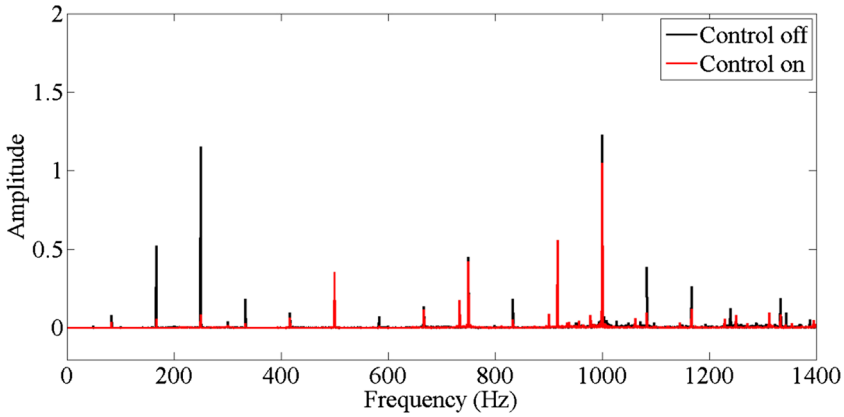

Fig. 15 The acceleration signals in frequency domain

chatter suppression. The rolling bearing and ring are mounted on the toolholder for transferring forces from piezoelectric stacks to toolholder. The real toolholder and machining set up are seen in Figs. 12 and 13.

3.2.3 Verification of control algorithm by contrast milling tests

The contrast milling tests are implemented with control or not. As seen Fig. 6, the parameters (5000 rpm, 3 mm) are located in the strongly unstable region, which can be selected as the milling parameters for chatter control. The radial cutting depth is 0.5 mm and the feed per tooth is 0.05 mm/tooth.

The time domain acceleration signals during milling process are as seen in Fig. 14, and the values of root-mean-square are 27.4 and 15.1 m/s^2, respectively, which means that the proposed control method can reduce the milling vibration by about 44.9%.

With the acceleration signals in the frequency domain as shown in Fig. 15, the milling vibration is mitigated in a large extent in the whole frequency range. Although the vibration increases at some points, for example, 500, 733.7, and 916.7 Hz, it does not affect the whole reduction of vibration amplitude at the most frequencies.

In addition to the vibration index, the surface quality of finished parts is also selected to evaluate the machining

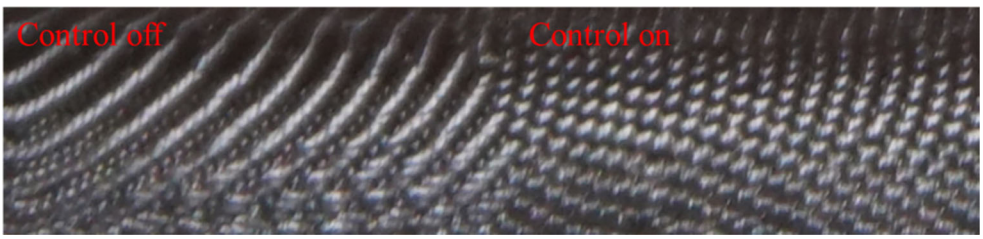

Fig. 16 The finished part surface

quality as seen in Fig. 16, which shows that the surface quality with control is better and verifies the effectiveness of the algorithm.

4 Conclusions

In this study, the milling dynamic equations are established based on the effect of tool bending and helix. In addition, the time-domain LMS adaptive algorithm is constructed and implemented for chatter suppression. According to the analysis and experiment results, the conclusions are as follows: (1) The milling tool, especially with the small diameter-overhang ratio, will bend due to the cutting forces. The flexural displacement and bending angle can be calculated with corresponding formulas. (2) In milling dynamic model, the tool bending will reduce the instantaneous cutting area, which will decrease the cutting forces and enlarge the stable region. Besides, the tool helix will cause the change in the angular position of tool teeth along the axial direction, which will also influence the calculation of the instantaneous cutting area. (3) The stability with tool bending and helix is analyzed using SDM, which is verified by a number of milling tests. (4) The smart toolholder equipped with piezoelectric stack actuators is designed and mounted to a three-axis milling machine, which can apply the control algorithm to experiments. (5) The time-domain LMS algorithm can suppress chatter effectively, which is validated by the contrast milling tests with control or not.

Funding information This work is supported by the National Natural Science Foundation of China (Nos. 51405370 and 51421004), the Project Funded by Key Laboratory of Product Quality Assurance & Diagnosis (No. 2014SZS14-P05), and the open foundation of Zhejiang Provincial Key Laboratory of Laser Processing Robot/Key Laboratory of Laser Precision Processing & Detection (lzsy-12).

References

1. Kayhan M, Budak E (2009) An experimental investigation of chatter effects on tool life. Proc Inst Mech Eng B J Eng Manuf 223(11): 1455–1463. https://doi.org/10.1243/09544054JEM1506
2. Taylor FW (1907) On the art of cutting metals. Trans ASME 28:31–58
3. Tobias SA (1965) Machine tool vibration. Blackie and Sons, London
4. Koenigsbeger F, Tlusty J (1970) Machine tool structures. Pergamon Press, Oxford
5. Altintas Y, Budak E (1995) Analytical prediction of stability lobes in milling. CIRP Ann Manuf Technol 44(1):357–362. https://doi.org/10.1016/S0007-8506(07)62342-7
6. Insperger T, Muñoa J, Zatarain M, Peigné G (2006) Unstable islands in the stability chart of milling processes due to the helix angle. CIRP 2nd International Conference on High Performance Cutting, Vancouver, Canada, pp 12–13
7. Schmitz TL, Couey J, Marsh E, Mauntler N, Hughes D (2007) Runout effect in milling: surface finish, surface location error and stability. Int J Mach Tools Manuf 47(5):841–851. https://doi.org/10.1016/j.ijmachtools.2006.06.014
8. Tang AJ, Liu ZQ (2009) Three-dimensional stability lobe and maximum material removal rate in end milling of thin-walled plate. Int J Adv Manuf Technol 43(1-2):33–39. https://doi.org/10.1007/s00170-008-1695-y
9. Tyler C, Schmitz T (2013) Analytical process damping stability prediction. J Manuf Process 15(1):69–76. https://doi.org/10.1016/j.jmapro.2012.11.006
10. Balachandran B (2001) Nonlinear dynamics of milling processes. Philos Trans R Soc Lond A 359(1781):793–819. https://doi.org/10.1098/rsta.2000.0755
11. Balachandran B, Zhao MX (2000) A mechanics based model for study of dynamics of milling operations. Meccanica 35(2):89–109. https://doi.org/10.1023/A:1004887301926
12. Long X, Balachandran B (2010) Stability of up-milling and down-milling operations with variable spindle speed. J Vibration Control 16(16):1151–1168. https://doi.org/10.1177/1077546309341131
13. Yang Y, Zhang WH, Ma YC, Wan M (2016) Chatter prediction for the peripheral milling of thin-walled workpieces with curved surfaces. Int J Mach Tools Manuf 109:36–48. https://doi.org/10.1016/j.ijmachtools.2016.07.002
14. Totis G (2017) Breakthrough of regenerative chatter modeling in milling by including unexpected effects arising from tooling system deflection. Int J Adv Manuf Technol 89(9–12):2515–2534. https://doi.org/10.1007/s00170-016-9855-y
15. Totis G, Albertelli P, Torta M, Sortino M, Monno M (2017) Upgraded stability analysis of milling operations by means of advanced modeling of tooling system bending. Int J Mach Tools Manuf 113C:19–34
16. Cao H, Zhang X, Chen X (2017) The concept and progress of intelligent spindles: a review. Int J Machine Tools Manuf 112:21–52. https://doi.org/10.1016/j.ijmachtools.2016.10.005
17. Dohner JL, Lauffer JP, Hinnerichs TD, Shankar N, Regelbrugge M, Kwan CM, Xu R, Winterb B (2004) Mitigation of chatter instabilities by active structural control. J Sound Vib 269(1-2):197–211. https://doi.org/10.1016/S0022-460X(03)00069-5
18. Van Dijk NJM (2011) Active chatter control in high-speed milling processes. Dissertation, Eindhoven University of Technology
19. Huang T, Chen Z, Zhang HT, Ding H (2015) Active control of an AMBs supported spindle for chatter suppression in milling process. J Dyn Syst Meas Control 137(11):111003. https://doi.org/10.1115/1.4030841
20. Monnin J, Kuster F, Wegener K (2014) Optimal control for chatter mitigation in milling—part 1: modeling and control design. Control Eng Pract 24:156–166. https://doi.org/10.1016/j.conengprac.2013.11.010
21. Monnin J, Kuster F, Wegener K (2014) Optimal control for chatter mitigation in milling—part 2: experimental validation. Control Eng Pract 24:167–175. https://doi.org/10.1016/j.conengprac.2013.11.011
22. Verschuren T (2009) Active chatter control in high-speed milling using μ-synthesis. Dissertation, Eindhoven University of Technology
23. Dijk NJM, Wouw N, Doppenberg EJJ, Oosterling JAJ, Nijmeijer H (2012) Robust active chatter control in the high-speed milling process. IEEE Trans Control Syst Technol 20(4):901–917. https://doi.org/10.1109/TCST.2011.2157160
24. Zhang HT, Wu Y, He DF, Zhao H (2015) Model predictive control to mitigate chatters in milling processes with input constraints. Int J

Mach Tools Manuf 91:54–61. https://doi.org/10.1016/j.ijmachtools.2015.01.002

25. Rashid A, Nicolescu CM (2006) Active vibration control in palletised workholding system for milling. Int J Mach Tools Manuf 46(12–13):1626–1636. https://doi.org/10.1016/j.ijmachtools.2005.08.020
26. Jia ZM, Xiang YK, Ji Huan GE, Nie WM (2017) Design and experimental study of cutting chatter control system based on filtered-X LMS. Mach Tool Hydraul 45(6):100–104. http://www.en.cnki.com.cn/Article_en/CJFDTotal-JCYY201706018.htm
27. Zhang X, Wang C, Gao RX, Yan R, Chen X, Wang S (2016) A novel hybrid error criterion-based active control method for on-line milling vibration suppression with piezoelectric actuators and sensors. Sensors 16(1):68. https://doi.org/10.3390/s16010068
28. Wang C, Zhang X, Liu Y, Cao H, Chen X (2018) Stiffness variation method for milling chatter suppression via piezoelectric stack actuators. Int J Mach Tools Manuf 124:53–66. https://doi.org/10.1016/j.ijmachtools.2017.10.002
29. Long XH, Balachandran B (2007) Stability analysis for milling process. Nonlinear Dyn 49(3):349–359. https://doi.org/10.1007/s11071-006-9127-8
30. Gross D, Ehlers W, Wriggers P, Schröder J, Müller R (2017) Mechanics of materials—formulas and problems. Springer, Berlin Heidelberg. https://doi.org/10.1007/978-3-662-53880-7
31. Altintas Y (2012) Manufacturing automation; metal cutting mechanics, machine tool vibrations and CNC design. Cambridge University Press, Cambridge
32. Stephenson DA, Agapiou JS (2016) Metal cutting theory and practice. CRC Press, Boca Raton. https://doi.org/10.1201/b19559
33. Insperger T, Stepan G (2004) Updated semi-discretization method for periodic delay-differential equations with discrete delay. Int J Numer Methods Eng 61(1):117–141. https://doi.org/10.1002/nme.1061